LAWRENCE
LIVERMORE
NATIONAL
LABORATORY

LLNL-JRNL-836059

Silicon photomultipliers coupled to scintillators with the emission maximum at 550 nm

F. Liang, H. Brands, L. Hoy, J. Smith, J. Verity, R. Wilson, N. Cherepy, S. O'Neal, S. Payne, Z. Seeley, T. Wineger

June 7, 2022

IEEE Transactions on Nuclear Science

Disclaimer

Silicon photomultipliers coupled to scintillators with the emission maximum at 550 nm

Felix Liang, *Senior Member, IEEE,* Hartmut Brands, *Member, IEEE,* Les Hoy, *Member, IEEE,* Jason Smith, *Member, IEEE,* Jeff Verity, Rick Wilson, Nerine J. Cherepy, *Senior Member, IEEE,* Sean P. O'Neal, Stephen A. Payne, *Member, IEEE,* Zachary M. Seeley, and Tyler J. Wineger

***Abstract*—A majority of the silicon photomultipliers (SiPMs) are sensitive to blue and near ultraviolet photons which are not optimized for scintillators with the emission maximum at wavelengths longer than 500 nm. The Red-Green-Blue (RGB) SiPM is developed for the maximum photon detection efficiency (PDE) at 550 nm which is a good match for some high-light-yield scintillators, such as CsI:Tl (CsI) and $Gd_{1.5}Y_{1.5}Ga_2Al_3O_{12}$:Ce (GYGAG). Comparisons are made for the performance of these scintillators coupled to the RGB SiPM and a blue-sensitive SiPM. Because it takes tens of nanoseconds for the microcells to recharge after registering a photon hit, the linearity of these scintillation detectors was studied for high energy gammas where numerous scintillation photons are generated. Additionally, the energy resolution of the 662 keV gamma emitted by ^{137}Cs was measured for temperatures between –20 and 50°C. The nonlinearity was observed above 1 MeV for all measurements, however, it can be corrected by energy calibration using a third-degree polynomial. For CsI, the energy resolution is better with the blue-sensitive SiPM because of the lower dark count rate. In contrast, GYGAG coupled to the RGB SiPM has a better energy resolution for temperatures below 30°C because of the well matched emission spectrum and PDE distribution. Nevertheless, the advantage disappears for temperatures above 30°C due to the higher dark count rate. It would be useful to further develop the RGB SiPM with a lower dark count rate and higher operating temperatures.**

***Index Terms*—silicon photomultiplier, cesium iodide, gadolinium yttrium gallium aluminum garnet, scintillation detector, gamma spectroscopy.**

I. Introduction

Photomultiplier tubes (PMT) have been the photosensor of choice for scintillation detectors for decades owing to their high gain, good quantum efficiency, low noise, and fast response. In recent years, the development of silicon photomultipliers (SiPMs), a solid-state photosensor, has progressed rapidly and SiPMs have become an alternative readout device for scintillation detectors in several applications. Similar to PMTs, SiPMs have high gain and good photon detection efficiency (PDE) which is suitable for coupled to scintillators for use in gamma spectroscopy [1], [2], [3]. In addition, SiPMs are compact, rugged, and of low voltage operation which are useful for making small form factor, lightweight, and low power detectors for security applications [4], [5], [6] and for detector modules deployed in space applications [7], [8], [9]. The insensitivity to magnetic fields of SiPMs allows the scintillation detectors in positron emission tomography (PET) scanners to function in conjunction with magnetic resonance imaging (MRI) for medical diagnosis [10], [11], [12]. Furthermore, the fast timing output of SiPMs enables time-of-flight measurements in PET which help improve image quality [13], [14].

The PDE maximum for a majority of SiPMs is located at 420 nm in wavelength, blue and near ultraviolet (NUV) in color. This is similar to PMTs which are a good match for the emission of a large number of scintillators such as NaI:Tl, $LaBr_3$:Ce, $CeBr_3$, $Cs_2LiLaBr_6$:Ce (CLLB), $Cs_2LiLaBr_{6-x}Cl_x$:Ce (CLLBC), Cs_2LiYCl_6:Ce (CLYC), $Lu_{1.8}Y_2SiO_5$:Ce (LYSO), and so on. However, there is a class of scintillators with the emission maximum at wavelengths longer than 500 nm such as CsI:Tl (CsI), $Lu_3Al_5O_{12}$:Ce (LuAG), $Gd_3Al_2Ga_3O_{12}$:Ce (GAGG), $Gd_{1.5}Y_{1.5}Ga_2Al_3O_{12}$:Ce (GYGAG), etc. Among them, CsI, GYGAG, and GAGG have high light yield, more than 50,000 photons/MeV, and are either slightly hydroscopic, the former, or nonhydroscopic at all, the latter two, which are easier to handle and more durable for deployment in scintillation detectors. In addition, it has been reported that GYGAG, a new scintillation material, is capable of achieving an energy resolution of 4% at 662 keV of ^{137}Cs which is useful for applications requiring detailed spectroscopy [15]. To address the mismatch of the blue-sensitive SiPM's PDE distribution with the emission spectrum of these scintillators, Fondazione Bruno Kessler (FBK, Trento, Italy) has developed SiPMs with the PDE maximum at a wavelength of 550 nm which are referred to as the Red-Green-Blue (RGB) SiPMs [16], [17], [18], [19].

In this paper, the performance of CsI and GYGAG coupled to the RGB SiPMs is compared with those coupled to the blue-sensitive SiPMs. Since both types of SiPMs have small microcells, high fill factor, and fast recharge time, the influence of high energy gammas on the linearity of scintillation detectors using these SiPMs will be examined. Moreover, the energy resolution dependence on the overvoltage for temperatures

Felix Liang, Hartmut Brands, Les Hoy, Jason Smith, Jeff Verity, and Rick Wilson are with Teledyne FLIR LLC., Oak Ridge, TN 37830, USA. (e-mail: felix.liang@teledyneflir.com)

Nerine J. Cherepy, Sean P. O'Neal, Stephen A. Payne, Zachary M. Seeley, and Tyler J. Wineger are with Lawrence Livermore National Laboratory, Livermore, CA 94551, USA.

This work was supported in part by the U.S. Department of Homeland Security, Countering Weapons of Mass Destruction Office under Award IAA HSHQDN-17-X-00016. This support does not constitute an express or implied endorsement on the part of the Government.

Work was performed under the auspices of the U.S. Department of Energy by Lawrence Livermore National Laboratory under Contract DE-AC52-07NA27344.

This document does not contain any export-controlled information.

between –20 and 50°C will be presented. In Section II, the scintillators, SiPMs, and data acquisition will be discussed. The measurement results and comparisons will be given in Section III, followed by conclusions in Section IV.

II. Experiment

A. Scintillator

The CsI crystal was a 25 mm×25 mm×16 mm square cuboid with all six surfaces polished. One of the 25 mm×25 mm surfaces was coupled to an array of SiPMs using an optical interface and the rest of the surfaces were wrapped with polytetrafluoroethylene (PTFE) tape. Since CsI is slightly hydroscopic, the crystal and the SiPM array were installed in a hermetically sealed aluminum box.

The GYGAG scintillator was a Ø24 mm×12 mm cylinder, also with all surfaces polished. It was fabricated using a pressing-and-sintering technique yielding a transparent ceramic [20]. The SiPM array was coupled to one of the circular surfaces and the rest of the surfaces were covered by PTFE tape. In order to maintain the same testing conditions and keep the ambient light from interfering with the measurement, the GYGAG scintillator and the SiPM array were also enclosed in the aluminum box.

Table I shows the physical properties of GYGAG and CsI [21], [22], [23]. The light yield, density, and effective Z (atomic number) for stopping gammas are high for both scintillators. Fig. 1 shows the emission spectra for GYGAG [21] and CsI [22] normalized at the maximum. The spectral shape is similar for both scintillators at wavelengths longer than the emission maximum. The emission of CsI is broader at the other side of the emission maximum whereas the emission of GYGAG does not extend to wavelength shorter than 460 nm because of the self-absorption by Ce [21].

TABLE I
PHYSICAL PROPERTIES OF GYGAG AND CSI.

	GYGAG	CsI
Light yield (photons/MeV)	50,000	54,000
Decay time (ns)	120 (34%)	600 (54%)
	890 (66%)	3400 (46%)
Peak emission wavelength (nm)	550	550
Refractive index	1.9	1.79
Density (g/cm^3)	5.8	4.51
Z_{eff}	48	54

B. Silicon Photomultiplier

As the largest SiPMs are smaller than the coupling surface of the scintillators, arrays of SiPMs were constructed. For the RGB SiPMs, nine 4 mm×4 mm SiPMs (First Sensor SiPM-RGB4S-SMD) were arranged in a 3×3 array resulting in a detection area of 12 mm×12 mm. Likewise, four blue-sensitive SiPMs (On Semiconductor MicroFJ-60035-TSV) each with dimensions of 6 mm×6 mm were used to build a 2×2 array which has the same detection area as the RGB SiPM array. For both arrays, the SiPMs were populated on a printed circuit board where the spacing between adjacent SiPMs was less than 1 mm. Since the coupling surface of both scintillators was larger than the footprint of the SiPM arrays, the overhang was covered with PTFE.

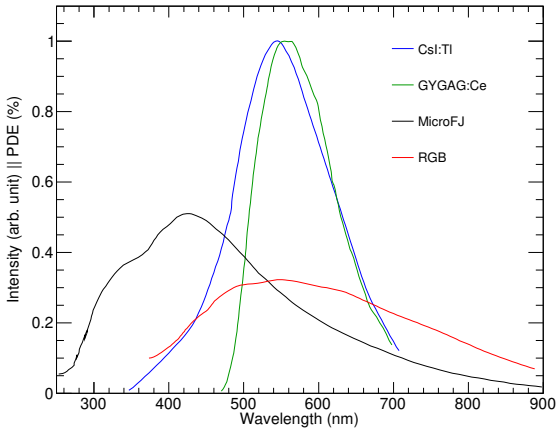

Fig. 1. The emission spectrum of GYGAG and CsI normalized to the emission maximum, and the photon detection efficiency of the RGB SiPM (First Sensor SiPM-RGB4S-SMD) and the blue sensitive SiPM (On Semiconductor MicroFJ-60035).

Table II shows some key parameters for the RGB and MicroFJ SiPMs and Fig. 1 shows the PDE at the maximum overvoltage (V_{OV}), bias above the breakdown voltage (V_{BD}), as a function of wavelength for the two types of SiPMs [24], [25]. At the emission maximum of GYGAG and CsI, 550 nm, the PDE is 32.5% for the RGB SiPM and 28% for the MicroFJ SiPM.

TABLE II
SELECTED PARAMETERS FOR RGB AND MICROFJ SIPMS.

	RGB	MicroFJ
Effective active area (mm^2)	4x4	6x6
Microcell size (μm)	40	35
Fill factor (%)	60	75
Breakdown voltage (Volt)	27	24.5
Overvoltage range (Volt)	2 to 4	1 to 6
Peak PDE wavelength (nm)	550	420
Peak PDE (%)	32.5	50
Gain at max V_{OV}	2.7x10^6	6.3x10^6
Dark count rate at max V_{OV} (kHz/mm^2)	200	150
Recharge time constant (ns)	50	50
Operating temperature range (°C)	–25 to 40	–40 to 85
Temperature dependence of V_{BD} (mV/°C)	27	21.5
Window refractive index	1.51	1.53

C. Measurement

Since the PDE of SiPMs changes with temperature, all measurements were performed with the detectors installed in a thermal chamber (Test Equity 115A). As required by the American National Standards Institute (ANSI) for radiation instruments, the measurements were carried out for temperatures between –20°C and 50°C [26]. However, the measurements with the RGB SiPMs were limited to the maximum operating temperature, 40°C, to avoid causing permanent damages to the SiPMs [24]. The measurements were performed at every 10°C above 20°C. For temperatures below 20°C the measurements

were performed at 0°C and −20°C because the dark count rate (DCR) of SiPMs is lower which has less influence on the energy resolution. During the change of chamber temperature, the ramping rate was 1°C every 8 minutes. At each temperature, the detectors were allowed at least 3 hours to equilibrate before experimentation.

The SiPM bias was provided by a power supply (Toellner 8852) and adjusted according to the temperature dependence on the breakdown voltage to compensate for the change in PDE. The output of the SiPM array was amplified by a homemade preamp and recorded by a waveform digitizer (CAEN DT5730B) which performed charge integration to obtain pulse height spectra. The charge integration time was determined by varying the gate width to find the best energy resolution. Because the pulse shape of the detector output correlates with the decay time constant of the scintillator and the capacitance of the SiPM array, it was found that an integration duration of 9 μs for CsI and 3 μs for GYGAG was required. It is worth pointing out that because of the higher dark count rate in the RGB SiPMs, to be discussed in Sect. III-B, the best energy resolution for CsI was observed with an integration time of 6 μs. However, the pulse height of the 662 keV gamma continued to increase steadily with longer integration times which suggests that the 6 μs gate was too short to capture the length of the pulse. Since the pulse shape output by both SiPMs coupled to CsI was very similar and the best energy resolution for CsI coupled to the MicroFJ SiPMs was obtained with an integration time of 9 μs, the RGB SiPMs also used the same integration time. The data acquired by the digitizer was stored on a PC for offline analysis.

III. Results and Discussion

A. Linearity

Fig. 2 shows the relative pulse height as a function of the energy for gamma peaks from ^{22}Na, ^{40}K, ^{57}Co, ^{60}Co, ^{133}Ba, ^{137}Cs, ^{152}Eu, and ^{232}Th sources. Since the non-proportionality of CsI occurs at energies below 500 keV [27] and the light yield of GYGAG decreases at energy below 500 keV [21], data are shown for energies above 500 keV. Furthermore, the energy calibration was performed using the data points of 511 keV of ^{22}Na and 662 keV of ^{137}Cs, assuming that the SiPM response is linear in this energy region. For higher gamma energies, the data points would follow the dashed line if the recovery time of the SiPM microcells is negligible comparing to the arrival times of multiple scintillation photons such that all the photons were detected by the microcells.

It can be seen that the data point for the 835 keV of ^{54}Mn is very close to the dashed line suggesting that the SiPM response is fairly linear between 511 and 662 keV. For energies above 1 MeV, the data points clearly deviate from the dashed line and the deviation is increasingly larger for higher gamma energies which is the result of the microcell's recharging time longer than the interval of consecutive photons arriving at the same microcell and the microcell stops responding before recovering.

The largest nonlinear response is observed for CsI coupled to the MicroFJ SiPMs which is attributed to the emission

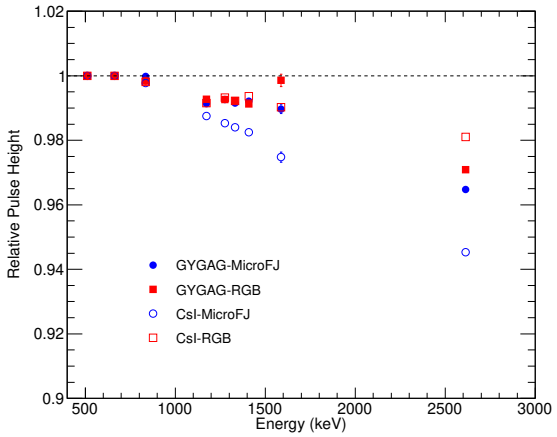

Fig. 2. Relative pulse height vs. energy for gamma peaks from ^{22}Na, ^{40}K, ^{54}Mn, ^{57}Co, ^{60}Co, ^{133}Ba, ^{137}Cs, ^{152}Eu, and ^{232}Th. The solid circles are for GYGAG coupled to the MicroFJ SiPMs, the solid squares for GYGAG coupled to the RGB SiPMs, the open circles for CsI coupled to the MicroFJ SiPMs, and the open squares for CsI coupled to the RGB SiPMs.

spectrum of CsI extending to wavelengths shorter than 500 nm where the PDE of the SiPMs is higher. To demonstrate the influence of this nonlinearity on the gamma spectrum, Fig. 3 shows the energy spectrum of ^{232}Th using the linear energy calibration obtained by the 511 and 622 keV data points comparing with that using a third-degree polynomial for energy calibration. Without the higher order corrections, the spectrum appears compressed at high energies due to the increasing deadtime of microcells arising from the arrival of a large number of scintillation photons. It is worth noting that even though a higher degree polynomial is required for energy calibration, the nonlinearity at high energies is less than 10% which does not significantly degrade the detector performance to the extent that the use of the MicroFJ SiPMs for CsI readout is prohibited.

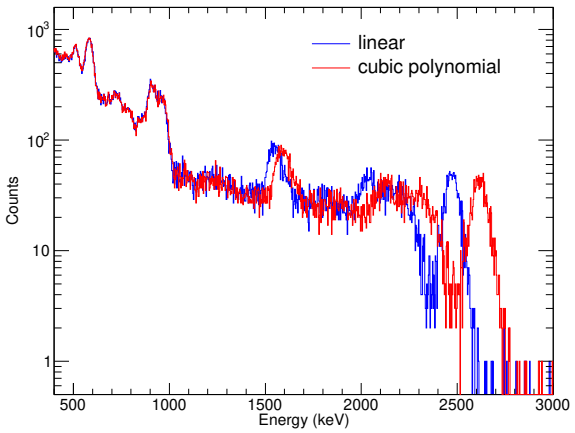

Fig. 3. Energy spectra of ^{232}Th measured by a 25 mm×25 mm×16 mm CsI coupled to the MicroFJ SiPM array. The blue spectrum is obtained with a linear energy calibration using the 511 keV of ^{22}Na and the 662 keV of ^{137}Cs data points and the red spectrum is obtained by using a third-degree polynomial for energy calibration.

Regardless of the broader emission spectrum of CsI at short wavelengths, the PDE for the RGB SiPMs is lower at short wavelengths. Therefore, some of these photons are not detected which gives the microcells a better chance to recharge leading to the smallest nonlinearity at 2.6 MeV.

While the emission spectrum of GYGAG is narrower and matches well with the wavelength dependence of PDE for the RGB SiPM, the nonlinear response of the SiPM is moderate. For the MicroFJ SiPMs, the PDE is lower than that of the RGB SiPMs and decreases toward longer wavelengths resulting in a mild nonlinear response, too. As shown in Fig 2, the nonlinearity is similar for GYGAG coupled to the RGB SiPMs and the MicroFJ SiPMs.

B. Energy Resolution for CsI

The energy resolution for the 662 keV gamma for CsI coupled to the RGB SiPM array with varying overvoltage for temperatures between –20 and 40°C is shown in Fig. 4. The overvoltages applied were 3.2, 3.5, and 3.8 V which correspond to 60%, 75%, and 90% of the operating range, respectively. The energy resolution improves steadily with increasing overvoltage except at 40°C where the energy resolution levels off above 3.5 V of overvoltage due to the increasing dark count rate. However, the best energy resolution observed at an overvoltage of 3.8 V is greater than 8% for all temperatures.

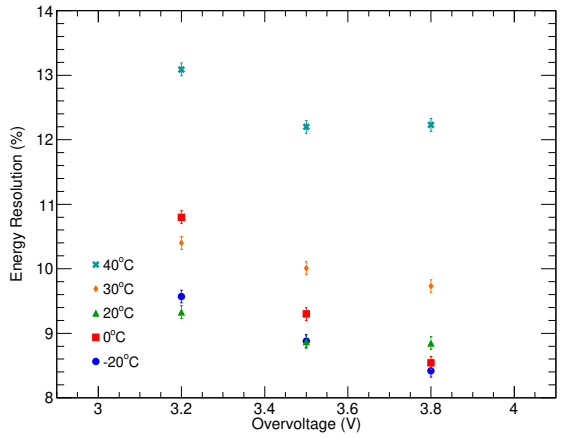

Fig. 4. Energy resolution for the 662 keV gamma of ^{137}Cs measured by CsI coupled to the RGB SiPM array as a function of overvoltage applied to the SiPMs. The measurements were performed at –20, 0, 20, 30, and 40°C.

Fig. 5 shows the energy resolution for the 662 keV gamma measured by CsI coupled to the MicroFJ SiPM array as a function of overvoltage applied to the SiPMs for temperatures between –20 and 50°C. The overvoltages applied to the SiPMs were 3, 3.75, and 4.5 V which correspond to 40%, 55%, and 70% of the operating range, respectively. The energy resolution improves with increasing overvoltage for temperatures below 40°C and the improvement becomes smaller at an overvoltage of 4.5 V. Because the dark count rate of SiPMs increases with temperature and overvoltage, the energy resolution is better at a lower overvoltage, 3.75 V, at 40 and 50°C. For temperatures between 0 and 30°C, energy resolution better than 6.5% can be achieved with overvoltages at and above 3.75 V. Due to the fact that the light yield for CsI is nearly constant between –55 and 50°C and a long decay time component becomes more prominent at low temperatures, it is necessary to use a longer integration time at low temperatures to capture all the scintillation photons [28]. Since the integration time is kept constant for all the temperatures, the poorer energy resolution observed at –20°C is likely the result of not capturing all of the photons in the long decay time component.

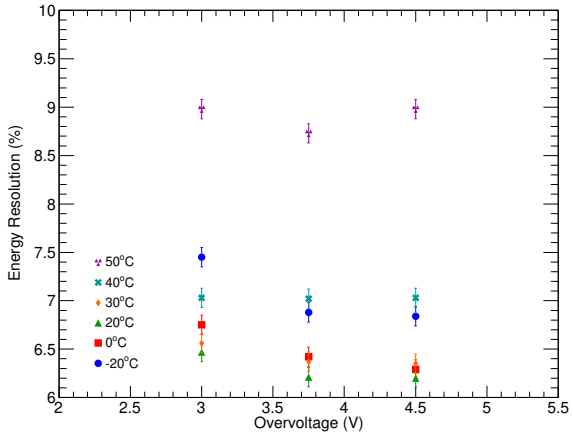

Fig. 5. Energy resolution for the 662 keV gamma of ^{137}Cs measured by CsI coupled to the MicroFJ SiPM array as a function of overvoltage applied to the SiPMs. The measurements were performed at –20, 0, 20, 30, 40, and 50°C.

The energy spectra for ^{137}Cs measured by CsI coupled to the RGB and the MicroFJ SiPMs at 20°C are compared in Fig. 6. Not only is the energy resolution for the 662 keV gamma better using the MicroFJ SiPMs, the 32 keV peak is also free from noise. Because the bias for the RGB SiPMs is at 90% of the operating range, the higher dark count rate resulted in noise creeping into the 32 keV peak. A comparison of the energy resolution of the 662 keV gamma measured by CsI coupled to the two SiPM arrays at 20°C as a function of integration time is presented in Fig. 7. For the MicroFJ SiPM array, the energy resolution deteriorates slightly for longer integration times. However, the energy resolution for the RGB SiPM array degrades appreciably with the integration time which manifests the impact of including more dark noise for longer integration times.

Fig. 8 presents the comparison of energy resolution for the 662 keV gamma measured by CsI coupled to the RGB and the MicroFJ SiPM arrays for temperatures from –20 to 40°C and to 50°C, respectively. The bias applied is 4.5 V above the breakdown voltage for the MicroFJ SiPMs and 3.8 V above the breakdown voltage for the RGB SiPMs. For the entire temperature range, using the MicroFJ SiPMs consistently show better energy resolution than using the RGB SiPMs even though the bias for the MicroFJ SiPMs is only 70% of the operating range comparing with the RGB SiPMs biased at 90% of the operating range.

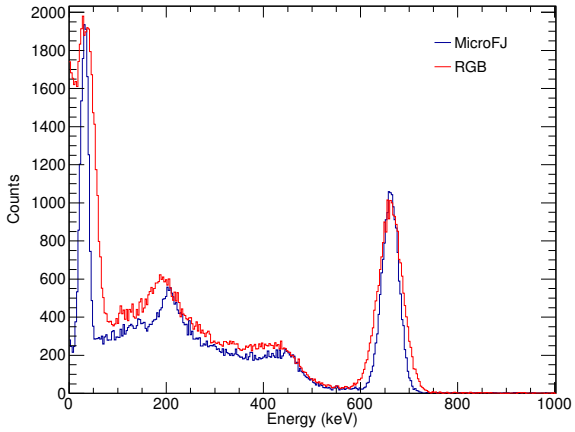

Fig. 6. Comparison of energy spectra of ^{137}Cs measured by CsI coupled to the MicroFJ SiPM array with that coupled to the RGB SiPM array measured at 20°C.

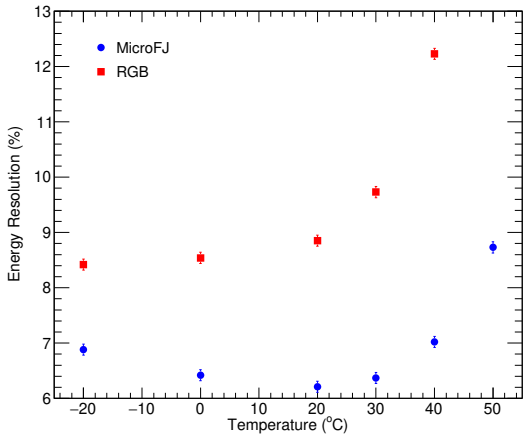

Fig. 8. Comparison of energy resolution for the 662 keV gamma of ^{137}Cs measured by CsI coupled to the MicroFJ and the RGB SiPM arrays for temperatures from –20 to 50°C and to 40°C, respectively.

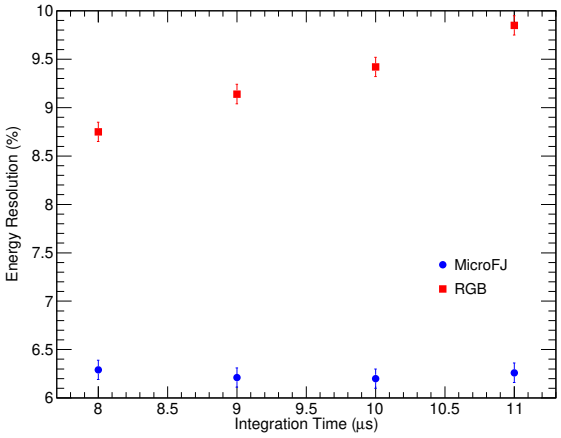

Fig. 7. Comparison of energy resolution of the 662 keV gamma measured by CsI coupled to the MicroFJ and RGB SiPM arrays at 20°C as a function of integration time.

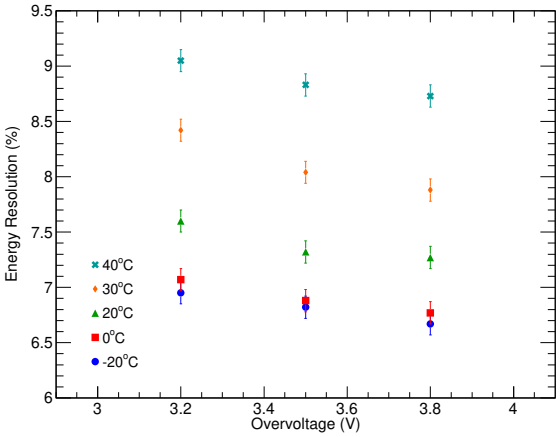

Fig. 9. Energy resolution for the 662 keV gamma of ^{137}Cs measured by GYGAG coupled to the RGB SiPM array as a function of overvoltage applied to the SiPMs. The measurements were performed at –20, 0, 20, 30, and 40°C.

C. Energy resolution for GYGAG

Fig. 9 shows the energy resolution for the 662 keV gamma of ^{137}Cs for GYGAG coupled to the RGB SiPM array with varying overvoltages for temperatures between –20 and 40°C. The same overvoltages as those in CsI coupled to the RGB SiPMs were used, 3.2, 3.5, and 3.8 V. The energy resolution improves steadily with increasing overvoltage even at 40°C unlike with CsI where the energy resolution levels off above 3.5 V of overvoltage. Although the best energy resolution achieved is 7.2% at 20°C, energy resolution better than 7% is observed at 0 and –20°C. When the same GYGAG scintillator was attached to a 2-inch PMT (Hamamatsu R6231), an energy resolution of 6% was observed. The poorer energy resolution obtained with the RGB SiPMs is attributed to the shape mismatch between the coupling surface of the scintillator and the SiPM array.

Since the coupling surface of CsI is a square, the overhang is homogeneous along the sides at which scintillation photons are reflected by PTFE. In contrast, the overhang for GYGAG is narrower near the corners of the SiPM array and wider near the middle of the array. Photons arriving near the edge of the coupling surface are collected by the SiPMs if they are near the corners of the array and are reflected if they are near the middle of the array. Consequently, the photon collection for GYGAG is less uniform which leads to poorer energy resolution.

The energy resolution for the 662 keV gamma measured by GYGAG coupled to the MicroFJ SiPM array as a function of overvoltage applied to the SiPMs for temperatures between –20 and 50°C is shown in Fig. 10. The same overvoltages as those for CsI were applied to the SiPMs, 3, 3.75, and 4.5 V. The energy resolution improves with increasing overvoltage for temperatures below 50°C. However, the best energy resolution achieved is above 7% even for temperatures below 20°C. By increasing the overvoltage to 4.75 and 5.5 V, 75% and 90% of the operating range, the energy resolution does not seem to improve. As a matter of fact, the best energy

resolution occurs for overvoltages between 4.5 and 4.75 V and higher bias voltages introduce a larger dark current which degrades the energy resolution.

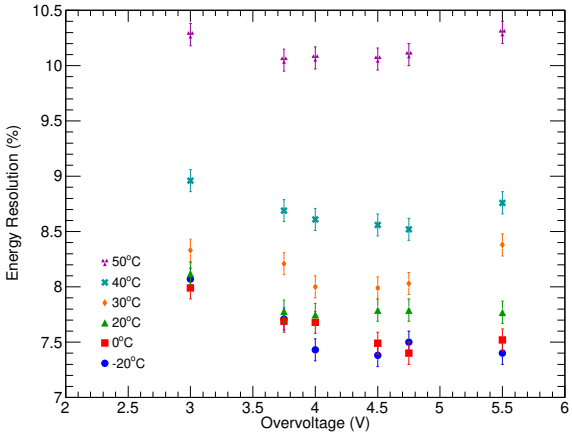

Fig. 10. Energy resolution for the 662 keV gamma of ^{137}Cs measured by GYGAG coupled to the MicroFJ SiPM array as a function of overvoltage applied to the SiPMs. The measurements were performed at –20, 0, 20, 30, 40, and 50°C.

Similar to using the RGB SiPM array, the shape mismatch of the coupling surface between GYGAG and the MicroFJ SiPM array contributes to the degradation of energy resolution. Moreover, by folding the PDE curves of the SiPMs with the emission spectrum of GYGAG in Fig. 1 to estimate the number of photons detected by the SiPMs shows that the MicroFJ SiPM collects 20% less photons than the RGB SiPM when the SiPMs are biased at the maximum overvoltage. Therefore, the narrower emission spectrum of GYGAG and the lower PDE of the MicroFJ SiPM at this wavelength range further contribute to reduce the performance. As a result, the energy resolution is poorer for GYGAG using the MicroFJ SiPMs as compared with using the RGB SiPMs.

The energy spectra for ^{137}Cs measured by GYGAG coupled to the RGB and the MicroFJ SiPMs at 20°C are compared in Fig. 11. Although the width of the 662 keV peak appears similar, the energy resolution is in fact slightly better for using the RGB SiPMs as shown in the inset of Fig. 11. It is 7.3% for the RGB SiPMs biased at 90% of the operating range and 7.8% for the MicroFJ SiPMs biased at 70% of the operating range.

For the 32 keV gamma, it is necessary to apply at least 1.2 V above the breakdown voltage, 60% of the operating range, for the RGB SiPMs to observe the peak. In contrast, the peak is already observable for the MicroFJ SiPMs with an overvoltage of 2 V, 40% of the operating range. In the figure, the peak amplitude for the 32 keV gamma is lower for the RGB SiPM which is owing to the higher ADC threshold that is required to remove the noise originated from the dark current.

Fig. 12 shows the comparison of energy resolution for the 662 keV gamma measured by GYGAG coupled to the RGB and the MicroFJ SiPM arrays for temperatures from –20 to 40°C and to 50°C, respectively. The bias applied is 3.8 V

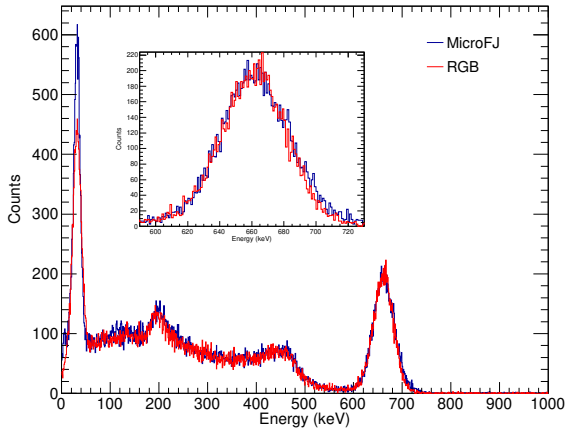

Fig. 11. Comparison of energy spectra of ^{137}Cs measured by GYGAG coupled to the MicroFJ SiPM array with that coupled to the RGB SiPM array measured at 20°C. The inset is a magnified view of the 662 keV peak.

above the breakdown voltage for the RGB SiPMs and 4.5 V above the breakdown voltage for the MicroFJ SiPMs. In spite of the better energy resolution for GYGAG using the RGB SiPMs than using the MicroFJ SiPMs for temperatures below 30°C, the difference is small compared to CsI where the energy resolution is significantly better for using the MicroFJ SiPMs. In addition, between –20 and 0°C the difference is nearly constant and it gets smaller as the temperature rises. For temperatures above 30°C, using the MicroFJ SiPMs for GYGAG readout yields a better energy resolution. The rapid degradation of energy resolution for using the RGB SiPM readout above 0°C suggests a fast rise of the dark count rate at these higher temperatures.

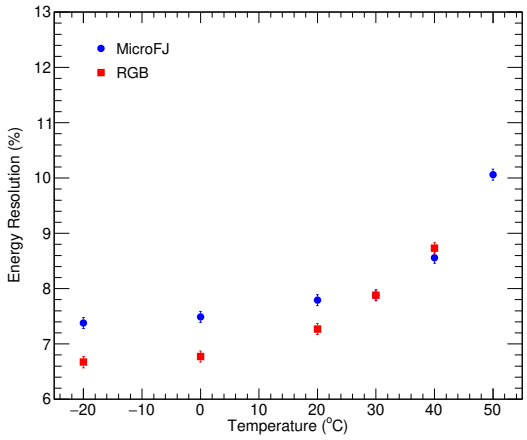

Fig. 12. Comparison of energy resolution for the 662 keV gamma of ^{137}Cs measured by GYGAG coupled to the MicroFJ and the RGB SiPM arrays for temperatures from –20 to 50°C and to 40°C, respectively.

Fig. 13 presents the pulse height, which is a measure of the light output, of the 662 keV gamma measured by GYGAG coupled to the MicroFJ SiPM array for temperatures between –20 and 50°C with respect to that at 20°C. At 50°C, the pulse

height is only 3% lower than that at 20°C whereas the pulse height at –20°C is 5.5% lower than that at 20°C. While the energy resolution measured by both SiPM arrays at 50°C is significantly worse than that at 20°C, the energy resolution at –20°C is similar to that at 20°C. This suggests that dark noise is the major source for the poorer energy resolution at high temperatures rather than the light output of GYGAG.

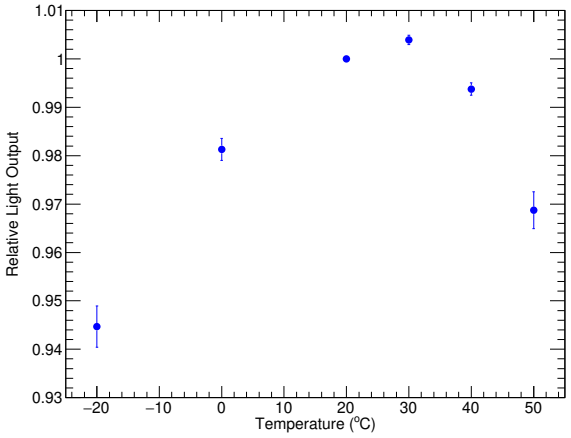

Fig. 13. Relative light output of GYGAG coupled to the MicroFJ SiPM array from –20 to 50°C.

IV. Conclusion

CsI and GYGAG coupled to the RGB SiPMs and the MicroFJ SiPMs all show small nonlinearity for high energy gammas. Since the relative pulse height at 2.6 MeV is at most 6% smaller than that at 662 keV, energy calibration using a third-degree polynomial is able to correct for the nonlinearity. For the CsI scintillator, because of its broader emission spectrum, particularly at shorter wavelengths, the MicroFJ SiPMs with a lower dark count rate results in a better energy resolution. In contrast, the emission spectrum of GYGAG and the wavelength dependence of PDE for the RGB SiPMs are a good match leading to the better energy resolution for temperatures below 30°C. The poorer energy resolution above 30°C is attributed to the higher dark count rate of the RGB SiPMs. Due to the requirements of detector usability under extreme environmental conditions, it would be beneficial to reduce the dark count rate and extend the operating temperature to at least 50°C for the RGB SiPMs.

References

[1] P. Buzhan, B. Dolgoshein, L. Filatov, A. Ilyin, V. Kantzerov, V. Kaplin, A. Karakash, F. Kayumov, S. Klemin, E. Popova, S. Smirnov, "Silicon photomultipliers and its possible applications", *Nucl. Instrum. Methods A*, vol. 504, pp. 48-52, 2003.

[2] C. Piemonte and A. Gola, "Overview on the main parameters and technology of modern silicon photomultipliers", *Nucl. Instrum. Methods A*, vol. 926, pp. 2-15, 2019.

[3] M. Grodzicka-Kobylka, M. Moszyński, T. Szczęśniak, "Silicon photomultipliers in gamma spectroscopy with scintillators", *Nucl. Instrum. Methods A*, vol. 926, pp. 129-147, 2019.

[4] M.P. Taggart, C. Payne, P.J. Sellin, "Neutron-gamma discrimination via PSD plastic scintillator and SiPMs", *J. of Phys: Conf. Ser.*, vol. 763, 012007, 2016.

[5] M.A. Wonders, A.M. Johnsen, C.C. Davison, S. Cheng, D.L. Chichester, M. Flaska, "Assessment of modern silicon photomultiplier radiation hardness in a nuclear security context", *2018 IEEE Nucl. Sci. Med. Imag. Conf. Proc. (NSS/MIC)*, (DOI: 10.1109/NSSMIC.2018.8824704).

[6] K. Kazkaz and T. Stiegler, "Replacing photomultiplier tubes with silicon photomultipliers for nuclear safeguards applications", *LLNL-TR-815543*, (DOI: 10.2172/1682525).

[7] P.F. Bloser, J.S. Legere, C. Bancroft, M.L. McConnell, J.M. Ryan, N. Schwadron, "Scintillator gamma-ray detectors with silicon photomultiplier readouts for high-energy astronomy", *Proc. SPIE 8859, UV, X-Ray, and Gamma-Ray Space Instrumentation for Astronomy XVIII*, 88590A, 2013.

[8] M. Casolino, G. Cambie, L. Marcelli, E. Reali, "SiPM development for space-borne and ground detectors: From Lazio-Sirad and Mini-EUSO to Lanfos", *Nucl. Instrum. Methods A*, vol. 986, 164649, 2021.

[9] L.J. Mitchell, B.F. Phlips, R.S. Woolf, T.T. Finne, A.L. Hutcheson, W. N. Johnson, M. Johnson-Rambert, R. Perea, "GAGG Radiation Instrumentation (GARI)", *Proc. SPIE 11821, UV, X-Ray, and Gamma-Ray Space Instrumentation for Astronomy XXII*, 1182105, 2021.

[10] D.P. McElroy, V. Saveliev, A. Reznik, J.A. Rowlands, "Evaluation of silicon photomultipliers: A promising new detector for MR compatible PET", *Nucl. Instrum. Methods A*, vol. 571, pp. 106-109, 2007.

[11] B. Weissler, P. Gebhardt, P.M. Dueppenbecker, J. Wehner, D. Schug, C.W. Lerche, B. Goldschmidt, A. Salomon, I. Verel, E. Heijman, M. Perkuhn, D. Heberling, R.M. Botnar, F. Kiessling, V. Schulz, "A digital preclinical PET/MRI insert and initial results", *IEEE Trans. Med. Imag.*, vol. 34, no. 11, pp. 2258-2270, 2015.

[12] D. Schug, C. Lerche, B. Weissler, P. Gebhardt, B. Goldschmidt, J. Wehner, P.M. Dueppenbecker, A. Salomon, P. Hallen, F. Kiessling, V. Schulz, "Initial PET performance evaluation of a preclinical insert for PET/MRI with digital SiPM technology", *Phys. Med. Biol.*, vol. 61, no. 7, pp. 2851-2878, 2016.

[13] A. Ronzhin, M. Albrow, S. Los, M. Martens, P. Murat, E. Ramberg, H. Kim, C.-T. Chen, C.-M. Kao, K. Niessen, A. Zatserklyaniy, M. Mazzillo, B. Carbone, G. Condorelli, G. Fallica, A. Piana, D. Sanfilippo, G. Valvo, S. Ritt, "A SiPM-based TOF-PET detector with high speed digital DRS4 readout", *Nucl. Instrum. Methods A*, vol. 703, pp. 109-113, 2013.

[14] S. Gundacker, R.M. Turtos, N. Kratochwil, R.H. Pots, M. Pagaoni, P. Lecoq, E. Auffray, "Experimental time resolution limits of modern SiPMs and TOF-PET detectors exploring different scintillators and Cerenkov emission", *Phys. Med. Biol.*, vol. 65, No. 2, 025001, 2020.

[15] E.L. Swanberg, N.J. Cherepy, B.M. Wihl, P.R. Beck, Z.M. Seeley, S.L. Hunter, S.E. Fisher, S.A. Payne, J. Kindem, "Transparent ceramic garnet gamma-ray spectrometer with directionality", *IEEE Trans. Nucl. Sci.*, vol. 65, No. 8, pp. 2303-2309, 2018.

[16] N. Serra, A. Ferri, A. Gola, T. Pro, A. Tarolli, N. Zorzi, C. Piemonte, "Characterization of new FBK SiPM technology for visible light detection", *JINST*, vol. 8, P03019, 2013.

[17] M. Grodzicka, M. Moszyński, T. Szczęśniak, A. Ferri, C. Piemonte, M. Szawłowski, A. Gola, K. Grodzicki, A. Tarolli, "Performance of FBK high-density SiPMs in scintillation spectrometry", *JINST*, vol. 12, P07001, 2017.

[18] V. Regazzoni, F. Acerbi, G. Cozzi, A. Ferri, C. Fiorini, G. Paternoster, C. Piemonte, D. Rucatti, G. Zappalà, N. Zorzi, A. Gola, "Characterization of high density SiPM non-linearity and energy resolution for prompt gamma imaging applications" *JINST*, vol. 9, P08004, 2014.

[19] F. Acerbi, G. Paternoster, M. Capasso, M. Marcante, A. Mazzi, V. Regazzoni, N. Zorzi, A. Gola, "Silicon photomultipliers: technology optimizations for ultraviolet, visible, and near-infrared range", *Instruments*, vol. 3, no. 1, 15, 2019.

[20] N.J. Cherepy, Z.M. Seeley, S.A. Payne, E.L. Swanberg, P.R. Beck, D.J. Schneberk, G. Stone, R. Perry, B.M. Wihl, S.E. Fisher, S.L. Hunter, P.A. Thelin, R.R. Thompson, N.M. Harvey, T. Stefanik, J. Kindem, "Transparent ceramic scintillators for gamma spectroscopy and MeV imaging", *Proc. SPIE 9593, Hard X-Ray, Gamma-Ray, and Neutron Detector Physics XVII*, 95930P, 2015.

[21] N.J. Cherepy, Z.M. Seeley, S.A. Payne, P.R. Beck, O.B. Drury, S.P. O'Neal, K. Morales Figueroa, S. Hunter, L. Ahle, P.A. Thelin, T. Stefanik, J. Kindem, "Development of transparent ceramic Ce-doped gadolinium garnet gamma spectrometers", *IEEE Trans. Nucl. Sci.*, vol. 60, no. 3, pp. 2330-2335, 2013.

[22] "CsI(Tl), CsI(Na) cesium iodide scintillation material", Accessed: 20 January 2022. [Online] Available: https://www.crystals.saint-gobain.com/sites/hps-mac3-cma-crystals/files/2021-09/CsITl-and-Na-Material-Data-Sheet.pdf

[23] P. Schotanus, R. Kamermans, P. Dorenbos, “Scintillation characteristics of pure and Tl-doped CsI crystals” *IEEE Trans. Nucl. Sci.*, vol. 37, no. 2, pp. 177-182, 1990.

[24] “Red, green, blue (RGB) SiPMs”, Accessed: 20 January 2022. [Online] Available: https://www.first-sensor.com/cms/upload/datasheets/SiPM-RGB_5000080-5000083.pdf

[25] “J-series SiPM Sensors”, Accessed: 20 January 2022. [Online] Available: https://www.onsemi.com/pdf/datasheet/microj-series-d.pdf

[26] “American national standard performance requirements for spectroscopic personal radiation detectors (SPRDs) for homeland security”, *ANSI N42.48-2018 (Revision of ANSI N42.48-2008)*, pp. 1-39, 2019;
“American nation standard performance criteria for handheld instruments for the detection and identification of radionuclides”, *ANSI N42.34-2015 (Revision of ANSI N42.48-2006)*, pp. 1-60, 2016.

[27] A. Syntfeld-Każuch, Ł. Świderski, W. Czarnacki, M. Gierlik, W. Klamra, M. Moszyński, P. Shotanus, “Non-proportionality and energy resolution of CsI(Tl)”, *IEEE Trans. Nucl. Sci.*, vol. 54, no. 5, pp. 1836-1841, 2007.

[28] J.D. Valentine, D.K. Wehe, G.F. Knoll, C.E. Moss, “Temperature dependence of CsI(Tl) absolute scintillation yield”, *IEEE Trans. Nucl. Sci.*, vol. 40, no. 4, pp. 1267-1274, 1993.